Collective transport for active matter run-and-tumble disk systems on a traveling-wave substrate

Cs. Sándor,[1,2] A. Libál,[1,2] C. Reichhardt,[1] and C. J. Olson Reichhardt[1]
[1]*Theoretical Division and Center for Nonlinear Studies, Los Alamos National Laboratory, Los Alamos, New Mexico 87545, USA*
[2]*Mathematics and Computer Science Department, Babeş-Bolyai University, Cluj 400084, Romania*
(Received 1 November 2016; published 17 January 2017)

We examine numerically the transport of an assembly of active run-and-tumble disks interacting with a traveling-wave substrate. We show that as a function of substrate strength, wave speed, disk activity, and disk density, a variety of dynamical phases arise that are correlated with the structure and net flux of disks. We find that there is a sharp transition into a state in which the disks are only partially coupled to the substrate and form a phase-separated cluster state. This transition is associated with a drop in the net disk flux, and it can occur as a function of the substrate speed, maximum substrate force, disk run time, and disk density. Since variation of the disk activity parameters produces different disk drift rates for a fixed traveling-wave speed on the substrate, the system we consider could be used as an efficient method for active matter species separation. Within the cluster phase, we find that in some regimes the motion of the cluster center of mass is in the opposite direction to that of the traveling wave, while when the maximum substrate force is increased, the cluster drifts in the direction of the traveling wave. This suggests that swarming or clustering motion can serve as a method by which an active system can collectively move against an external drift.

DOI: 10.1103/PhysRevE.95.012607

I. INTRODUCTION

Collections of interacting self-motile objects fall into the class of systems known as active matter [1,2], which can be biological in nature, such as swimming bacteria [3] or animal herds [4], a social system such as pedestrian or traffic flow [5], or a robotic swarm [6,7]. There are also a wide range of artificial active matter systems such as self-propelled colloidal particles [8–10]. Studies of these systems have generally focused on the case in which the motile objects interact with either a smooth or a static substrate; however, the field is now advancing to a point where it is possible to ask how such systems behave in more complex static or dynamic environments.

One subclass of active systems is a collection of interacting disks that undergo either run-and-tumble [11,12] or driven diffusive [13–15] motion. Such systems have been shown to exhibit a transition from a uniform density liquid state to a motility-induced phase-separated state in which the disks form dense clusters surrounded by a low-density gas phase [9–18]. Recently, it was shown that when phase-separated run-and-tumble disks are coupled to a random pinning substrate, a transition to a uniform density liquid state occurs as a function of the maximum force exerted by the substrate [19]. In other studies of run-and-tumble disks driven over an obstacle array by a dc driving force, the onset of clustering coincides with a drop in the net disk transport since a large cluster acts like a rigid object that can only move through the obstacle array with difficulty; in addition, it was shown that the disk transport was maximized at an optimal activity level or disk running time [20]. Studies of flocking or swarming disks that obey modified Vicsek models of self-propulsion [21] interacting with obstacle arrays indicate that there is an optimal intrinsic noise level at which collective swarming occurs [22,23], and that transitions between swarming and nonswarming states can occur as a function of increasing substrate disorder [24]. The dynamics in such swarming models differ from those of the active disk systems, so it is not clear whether the same behaviors will occur across the two different systems.

A number of studies have already considered overdamped active matter such as bacteria or run-and-tumble disks interacting with periodic obstacle arrays [25] or asymmetric arrays [26–29]. Self-ratcheting behavior occurs for the asymmetric arrays when the combination of broken detailed balance and the substrate asymmetry produces directed or ratcheting motion of the active matter particles [30,31], and it is even possible to couple passive particles to the active matter particles in such arrays in order to shuttle cargo across the sample [29]. In the studies described above, the substrate is static, and external driving is introduced via fluid flow or chemotactic effects; however, it is also possible for the substrate itself to be dynamic, such as in the case of time-dependent optical traps [32,33] or a traveling-wave substrate. Theoretical and experimental studies of colloids or cells in traveling-wave potentials reveal a rich variety of dynamical phases, self-assembly behaviors, and directed transport [34–41].

Here we examine a two-dimensional system of run-and-tumble active matter disks that can exhibit motility-induced phase separation interacting with a periodic quasi-one-dimensional (Q1D) traveling-wave substrate. In the low activity limit, the substrate-free system forms a uniform liquid state, while in the presence of a substrate, the disks are readily trapped by the substrate minima and swept through the system by the traveling wave. As the activity increases, a partial decoupling transition of the disks and the substrate occurs, producing a drop in the net effective transport. This transition is correlated with the onset of the phase-separated state, in which the clusters act as large-scale composite objects that cannot be transported as easily as individual disks by the traveling wave. We also find that the net disk transport is optimized at particular traveling-wave speeds, disk run length, and substrate strength. In the phase-separated state, we observe an interesting effect where the center of mass of each cluster moves in the direction opposite to that in which the traveling wave is moving, and we also find reversals to states in which the clusters and the traveling wave move in the same direction.

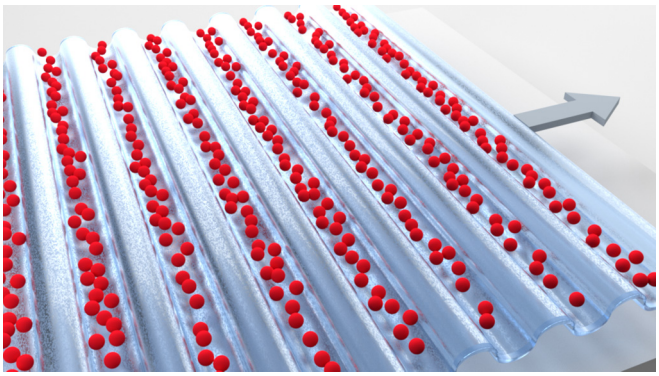

FIG. 1. Schematic of the system. Red spheres represent the active run-and-tumble disks in a two-dimensional system interacting with a periodic Q1D traveling-wave potential that is moving in the positive x-direction (arrow) with a wave speed of v_w.

The reversed motion of the clusters arises due to asymmetric growth and shrinking rates on different sides of the cluster. The appearance of backward motion of the cluster center of mass suggests that certain biological or social active systems can move against biasing drifts by forming large collective objects or swarms.

II. SIMULATION

We model a two-dimensional system of N run-and-tumble disks interacting with a Q1D traveling-wave periodic substrate, as shown in the schematic in Fig. 1 where the substrate moves to the right at a constant velocity v_w. The dynamics of each disk is governed by the following overdamped equation of motion:

$$\eta \frac{d\mathbf{r}_i}{dt} = \mathbf{F}_i^{\rm inter} + \mathbf{F}_i^m + \mathbf{F}_i^s, \tag{1}$$

where the damping constant is $\eta = 1.0$. Here the net velocity of disk i produced by self-propulsion, disk-disk interaction, and substrate forces is $d\mathbf{r}_i/dt$. The disk-disk repulsive interaction force $\mathbf{F}_i^{\rm inter}$ is modeled as a harmonic spring, $\mathbf{F}_i^{\rm inter} = \sum_{j\neq i}^{N} \Theta(d_{ij} - 2R)k(d_{ij} - 2R)\hat{\mathbf{d}}_{ij}$, where $R = 1.0$ is the disk radius, $d_{ij} = |\mathbf{r}_i - \mathbf{r}_j|$ is the distance between disk centers, $\hat{\mathbf{d}}_{ij} = (\mathbf{r}_i - \mathbf{r}_j)/d_{ij}$, and the spring constant $k = 20.0$ is large enough to prevent significant disk-disk overlap under the conditions we study yet small enough to permit a computationally efficient time step of $\delta t = 0.001$ to be used. We consider a sample of size $L \times L$ with $L = 300$, and we describe the disk density in terms of the area coverage $\phi = N\pi R^2/L^2$. The run and tumble self-propulsion is modeled with a motor force $\mathbf{F}_i^m$ of fixed magnitude $F^m = 1.0$ that acts in a randomly chosen direction during a run time of $\tilde{t}_r$. After this run time, the motor force instantly reorients into a new randomly chosen direction for the next run time. We take $\tilde{t}_r$ to be uniformly distributed over the range $[t_r, 2t_r]$, using run times ranging from $t_r = 1 \times 10^3$ to $t_r = 3 \times 10^5$. For convenience, we describe the activity in terms of the run length $r_l = F^m t_r \delta t$, which is the distance a disk would move during a single run time in the absence of a substrate or other disks. The substrate is modeled as a time-dependent sinusoidal force, $F_i^s(t) = A_s \sin(2\pi x_i/a - v_w t)$, where A_s is the substrate strength and x_i is the x position of disk i. We take a substrate periodicity of $a = 15$ so that the system contains 20 minima. The substrate travels at a constant velocity of v_w in the positive x-direction. We measure the average drift velocity of the disks in the direction of the traveling wave, $\langle V \rangle = N^{-1} \sum_i^N \mathbf{v}_i \cdot \hat{\mathbf{x}}$. We vary the run length, substrate strength, disk density, and wave speed. In each case, we wait for a fixed time of 5×10^6 simulation time steps before taking measurements to avoid any transient effects.

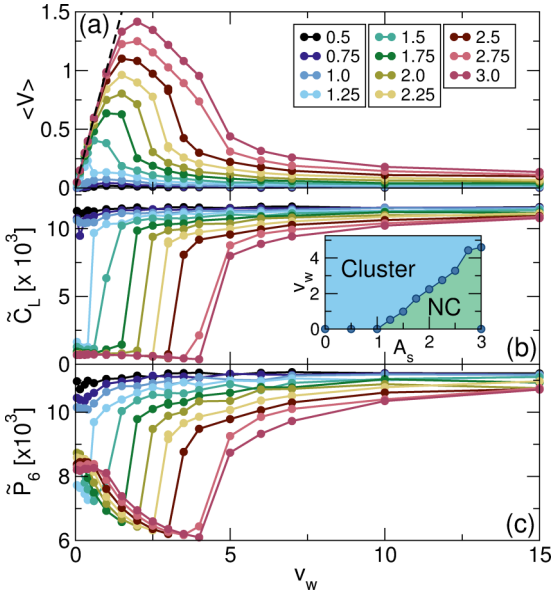

FIG. 2. (a) The average velocity per disk $\langle V \rangle$ vs wave speed v_w for a system with $N = 13\,000$ disks, $\phi = 0.453\,76$, and $r_l = 300$ for varied substrate strengths of $A_s = 0.5$ to 3.0. The dashed line indicates the limit in which all the disks move at the wave speed, $\langle V \rangle = v_w$. (b) The corresponding number $\tilde{C}_L$ of disks that are in a cluster vs wave speed. The inset shows the regions of cluster and noncluster (NC) states as a function of v_w vs A_s. (c) The number $\tilde{P}_6$ of sixfold-coordinated disks vs wave speed v_w.

III. RESULTS

In Fig. 2(a) we plot the average velocity per disk $\langle V \rangle$ versus wave speed v_w at different substrate strengths A_s for a system containing $N = 13\,000$ active disks, corresponding to $\phi = 0.453\,76$, at $r_l = 300$, a running length at which the substrate-free system forms a phase-separated state. The number of disks that are in the largest cluster, $\tilde{C}_L$, serves as an effective measure of whether the system is in a phase-separated state or not. We measure $\tilde{C}_L$ using the cluster identification algorithm described in Ref. [42], which identifies all disks that are in force contact with a given disk, a well-defined quantity. Once all force contact clusters have been identified, it is straightforward to pick out the largest cluster by simple disk counting. We call the system phase-separated when $\tilde{C}_L/N > 0.55$. In Fig. 2(b), we plot $\tilde{C}_L$ versus v_w at varied A_s, and in Fig. 2(c) we show the corresponding number of sixfold-coordinated disks, $\tilde{P}_6 = \sum_i^N \delta(z_i - 6)$, where z_i is the coordination number of disk i determined from a Voronoi construction [43]. In phase-separated states, most of the disks

within a cluster have $z_i = 6$ due to the triangular ordering of the densely packed state. In Fig. 2(a), the linearly increasing dashed line denotes the limit in which all the disks move with the substrate so that $\langle V \rangle = v_w$. At $A_s = 3.0$, $\langle V \rangle$ initially increases linearly, following the dashed line, up to $v_w = 1.25$, indicating that there is a complete locking of the disks to the substrate. For $v_w > 1.25$, there is a slipping process in which the disks cannot keep up with the traveling wave and jump to the next well. A maximum in $\langle V \rangle$ appears near $v_w = 2.0$, and there is a sharp drop in $\langle V \rangle$ near $v_w = 5.0$, which also coincides with a sharp increase in $\tilde{C}_L$ and $\tilde{P}_6$. The $\langle V \rangle$ versus v_w curves for $A_s > 1.0$ all show similar trends, with a sharp drop in $\langle V \rangle$ accompanied by an increase in $\tilde{C}_L$ and $\tilde{P}_6$, showing that the onset of clustering results in a sharp decrease in $\langle V \rangle$. For $A_s \leqslant 1.0$, the substrate is weak enough that the system remains in a cluster state even at $v_w = 0$, indicating that a transition from a cluster to a noncluster state can also occur as a function of substrate strength. In the inset of Fig. 2(b), we show the regions in which clustering and nonclustering states appear as a function of v_w versus A_s. At $v_w = 0$, there is a substrate-induced transition from a cluster to a noncluster state near $A_s = 1.0$, while for higher A_s, the location of the transition shifts linearly to higher v_w with increasing A_s. Since the motor force is $F^m = 1.0$, when $A_s < 1.0$ individual disks can escape from the substrate minima, so provided that r_l is large enough, the disks can freely move throughout the entire system and form a cluster state. For $A_s > 1.0$, the disks are confined by the substrate minima, but when v_w becomes large enough, the disks can readily escape the minima and again form a cluster state.

To highlight the correlation between the changes in the transport and the onset of clustering, in Figs. 3(a) and 3(b) we plot $\langle V \rangle / v_w$ and the normalized $C_L = \tilde{C}_L / N$ versus A_s at a fixed value of $v_w = 0.6$ from the system in Fig. 2. Here the cluster-to-noncluster transition occurs at $A_s = 1.25$, as indicated by the drop in C_L, which also coincides with a jump in $\langle V \rangle / v_w$. For this value of v_w, a complete locking between the disks and the traveling wave occurs for $A_s \geqslant 3.0$, where $\langle V \rangle / v_w = 1.0$. In Figs. 3(c) and 3(d) we plot $\langle V \rangle / v_w$ and C_L versus A_s for the same system at $v_w = 2.0$, where the cluster-to-noncluster transition occurs at a higher value of $A_s = 2.0$. This transition again coincides with a sharp increase in $\langle V \rangle / v_w$. In Fig. 4(a), we show images of the disk configurations for the system in Figs. 3(a) and 3(b) with $v_w = 0.6$ at $A_s = 0.75$, where the disks form a cluster state, while in Fig. 4(b), at $A_s = 2.5$ in the same system, the clustering is lost and the disks are strongly trapped in the substrate minima, forming chainlike states that move with the substrate. These results indicate that the clusters act as composite objects that only weakly couple to the substrate.

We next examine the case with a fixed substrate strength of $A_s = 2.0$ and varied r_l. Figure 5(a) shows $\langle V \rangle$ versus r_l for v_w values ranging from $v_w = 0.25$ to 6.0, and Fig. 5(b) shows the corresponding $\tilde{C}_L$ versus r_l. For $v_w < 3.0$, the system remains in a noncluster state for all values of r_l, while for $v_w \geqslant 3.0$

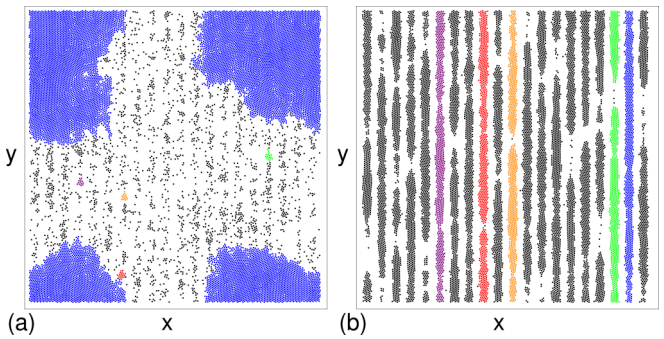

FIG. 4. The real-space positions of the active disks for the system in Figs. 3(a) and 3(b) with $v_w = 0.6$. (a) At $A_s = 0.75$, a phase-separated state appears. (b) At $A_s = 2.5$, the disks are strongly localized in the substrate minima and move with the substrate.

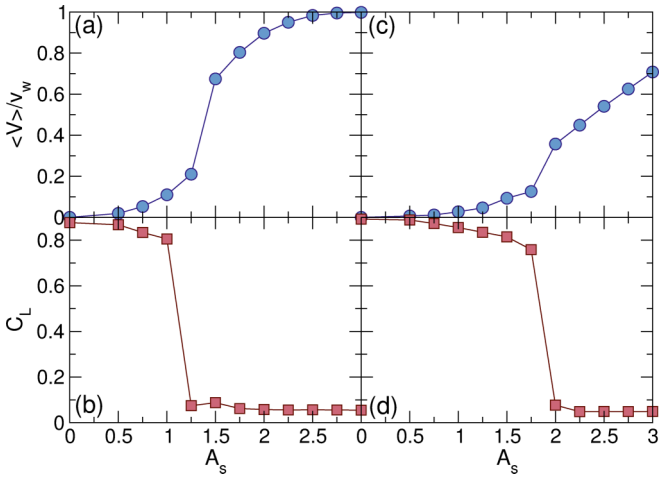

FIG. 3. (a) $\langle V \rangle / v_w$ vs A_s for the system in Fig. 2 at $v_w = 0.6$. (b) The corresponding normalized C_L showing that the transition from a cluster to a noncluster state coincides with an increase in $\langle V \rangle / v_w$. (c) $\langle V \rangle / v_w$ vs A_s for the same system with $v_w = 2.0$ where the cluster-to-noncluster transition occurs at a higher value of A_s. (d) The corresponding normalized C_L vs A_s.

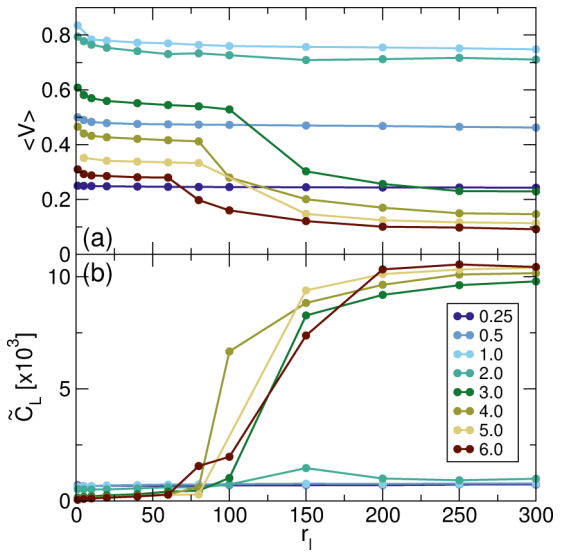

FIG. 5. (a) $\langle V \rangle$ vs r_l in samples with $A_s = 2.0$ and $\phi = 0.453$ for varied v_w from $v_w = 0.25$ to $v_w = 6.0$. (b) The corresponding $\tilde{C}_L$ vs r_l.

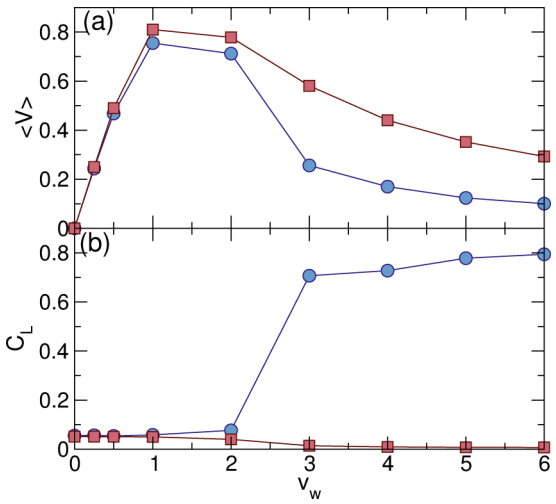

FIG. 6. A sample with $A_s = 2.0$ and $\phi = 0.453$ for $r_l = 5$ (red squares) and $r_l = 200$ (blue circles). (a) $\langle V \rangle$ vs v_w. (b) C_L vs v_w.

there is a transition from a noncluster to a cluster state with increasing r_l as indicated by the simultaneous drop in $\langle V \rangle$ and increase in $\tilde{C}_L$. In Figs. 6(a) and 6(b) we plot $\langle V \rangle$ and C_L versus v_w at $A_s = 2.0$ for $r_l = 200$ and 5.0. The system is in a noncluster state for all v_w when $r_l = 5.0$, and there is a peak in $\langle V \rangle$ near $v_w = 1.0$, while for $r_l = 200$ there is a transition to a cluster state close to $v_l = 3.0$, which coincides with a drop in $\langle V \rangle$ that is much sharper than the decrease in $\langle V \rangle$ with increasing v_w for the $r_l = 5$ system. In general, when r_l is small, the net transport of disks through the sample is greater than in samples with larger r_l. The fact that the net disk transport varies with varying r_l suggests that traveling-wave substrates could be used as a method for separating different types of active matter, such as clustering and nonclustering species.

When we vary the disk density ϕ while holding r_l fixed, we find results similar to those described above. In Fig. 7(a), we plot $\langle V \rangle$ versus v_w at $\phi = 0.56$ for varied A_s from $A_s = 0.5$ to 4.0, where we find a similar trend in which $\langle V \rangle$ increases with increasing wave speed when the disks are strongly coupled to the substrate. A transition to a cluster state occurs at higher v_w as shown in Fig. 7(b), where we plot $\tilde{C}_L$ versus v_w for the same samples. The increase in $\tilde{C}_L$ at the cluster state onset coincides with a drop in $\langle V \rangle$. In Fig. 7(c), we plot $\langle V \rangle$ versus ϕ for a system with fixed $v_w = 2.0$, $A_s = 2.5$, and $r_l = 300$, while in Fig. 7(d) we show the corresponding $\tilde{C}_L$ and $\tilde{P}_6$ versus ϕ. A transition from the noncluster to the cluster state occurs near $\phi = 0.6$, which correlates with a sharp drop in $\langle V \rangle$ and a corresponding increase in $\tilde{C}_L$ and $\tilde{P}_6$.

In Fig. 8(a) we show the disk configurations from the system in Fig. 7(a) at $A_s = 4.0$ and $v_w = 1.0$. Here $\langle V \rangle / v_w = 0.998$, indicating that the disks are almost completely locked with the traveling-wave motion and there is little to no slipping of the disks out of the substrate minima. In Fig. 8(b), the same system at $A_s = 2.0$ and $v_w = 1.5$ has a transport efficiency of $\langle V \rangle / v_w = 0.41$. No clustering occurs, but there are numerous disks that slip as the traveling wave moves. At $A_s = 1.0$ and $v_w = 0.6$ in Fig. 8(c) there is a low transport efficiency of $\langle V \rangle / v_w = 0.078$. The system forms a cluster state, and

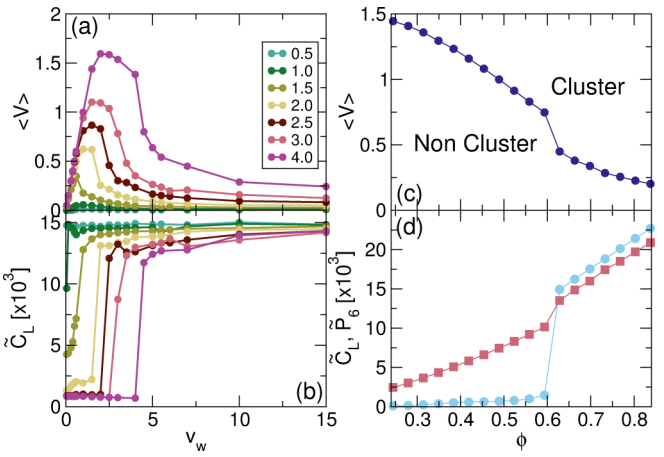

FIG. 7. (a) $\langle V \rangle$ vs v_w at $\phi = 0.56$ and $r_l = 300$ for varied $A_s = 0.5$ to 4.0. (b) The corresponding $\tilde{C}_L$ vs v_w. (c) $\langle V \rangle$ vs ϕ for $A_s = 2.5$, $r_l = 300$, and $v_w = 2.0$. (d) The corresponding $\tilde{C}_l$ (blue circles) and $\tilde{P}_6$ (red squares) vs ϕ where the onset of clustering occurs near $\phi = 0.6$ at the same point for which there is a drop in $\langle V \rangle$ in panel (c).

smaller numbers of individual disks outside of the cluster are transported by the traveling wave.

IV. FORWARD AND BACKWARD CLUSTER MOTION

In general, we find that when the traveling wave is moving in the positive x-direction, $\langle V \rangle > 0$; however, within the

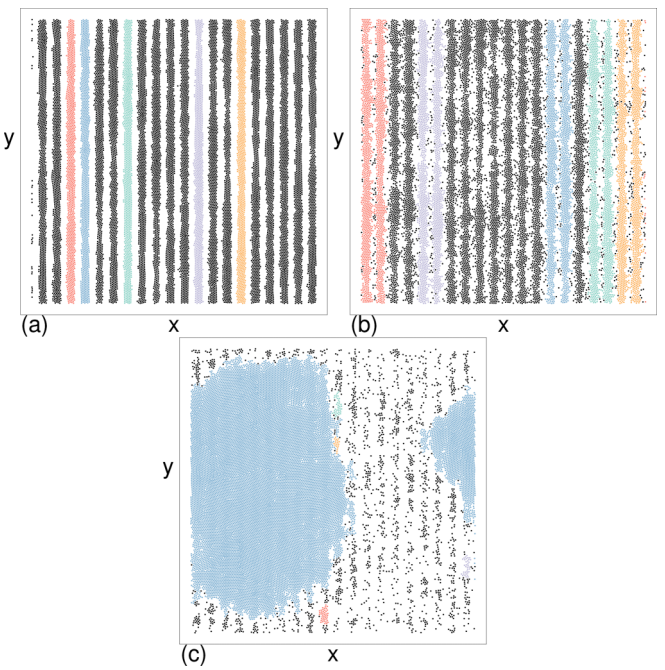

FIG. 8. The disk positions on the traveling-wave substrate for the system in Fig. 7(a) at $\phi = 0.56$. Colors indicate disks belonging to the five largest clusters. (a) Complete locking at $A_s = 4.0$ and $v_w = 1.0$, where the transport efficiency is $\langle V \rangle / v_w = 0.998$. (b) Partial locking at $A_s = 2.0$ and $v_w = 1.5$, where $\langle V \rangle / v_w = 0.41$. (c) Weak locking at $A_s = 1.0$ and $v_w = 0.6$ with $\langle V \rangle / v_w = 0.078$.

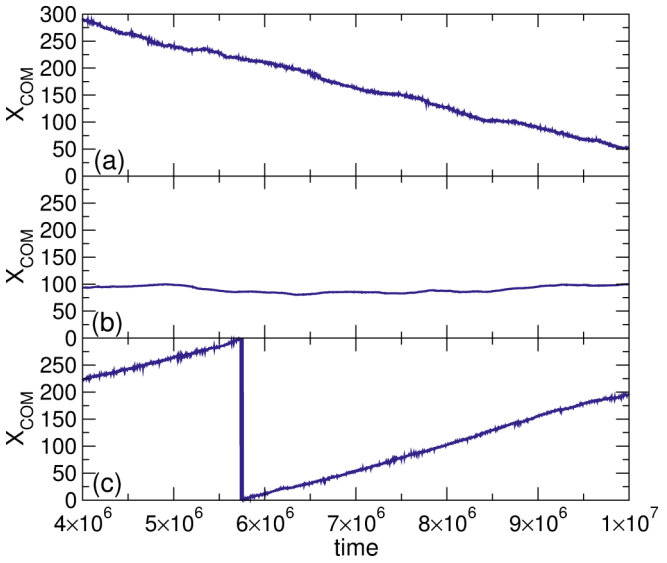

FIG. 9. The center-of-mass X_{COM} location of a cluster vs time in simulation time steps for a system with $\phi = 0.454$ and $r_l = 300$. (a) At $A_s = 1.25$ and $v_w = 0.6$, the cluster moves in the negative x-direction, against the direction of the traveling wave. (b) At $A_s = 0.5$ and $v_w = 4.0$, the cluster is stationary. (c) At $A_s = 3.0$ and $v_w = 7.0$, the cluster moves in the positive x-direction, with the traveling wave. The dip indicates the point at which the center of mass passes through the periodic boundary conditions.

cluster phase, the center-of-mass motion of a cluster can be in the positive or negative x-direction or the cluster can be almost stationary. By using the cluster algorithm to identify the location of the cluster center of mass, we can track the x-direction motion of the cluster center of mass X_{COM} over fixed time periods, as shown in Fig. 9(a) for a system with $\phi = 0.454$, $r_l = 300$, $A_s = 1.25$, and $v_w = 0.6$. During the course of 6×10^6 simulation time steps, the cluster moves in the negative x-direction a distance of 235 units, corresponding to a space containing 16 potential minima. Even though the net disk flow is in the positive x-direction, the cluster itself drifts in the negative x-direction. In Fig. 9(b) at $A_s = 0.5$ and $v_w = 4.0$, the disks are weakly coupled to the substrate and the cluster is almost completely stationary. Figure 9(c) shows that at $A_s = 3.0$ and $v_w = 7.0$, the cluster center-of-mass motion is now in the positive x-direction, and the cluster translates a distance equal to almost 20 substrate minima during the time period shown. The apparent dip in the center-of-mass motion is due to the periodic boundary conditions.

We have conducted a series of simulations and measured the direction and amplitude $V_{\mathrm{COM}} = dX_{\mathrm{COM}}/dt$ of the center-of-mass motion, as plotted in Fig. 10 as a function of A_s versus wave speed for the system in Fig. 7. The gray area indicates a region in which clusters do not occur, and in general we find that the negative cluster motion occurs at lower wave speeds while the positive motion occurs for stronger substrates and higher wave speeds. There are two mechanisms that control the cluster center-of-mass motion. The first is the motion of the substrate itself, which drags the cluster in the positive x-direction, and the second is the manner in which the cluster grows or shrinks on its positive x and negative x sides. At

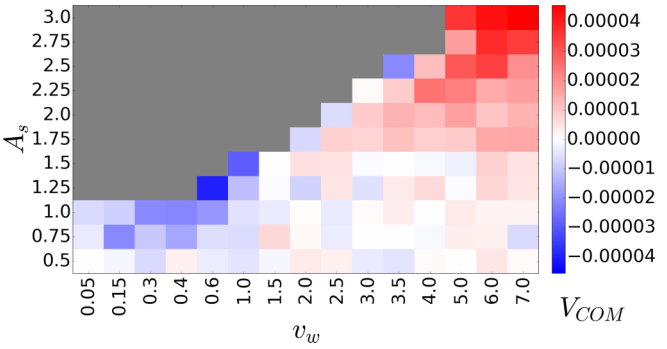

FIG. 10. Height field of the direction and magnitude of the center-of-mass motion in the x direction, V_{COM}, as a function of A_s vs v_w for the cluster obtained after 4×10^6 simulation steps. The gray area indicates a regime in which there is no cluster formation.

lower substrate strengths and low wave speeds, the disks in the cluster are weakly coupled to the substrate so the cluster does not move with the substrate. In this case, the disks can leave or join the cluster anywhere around its edge; however, disks tend to join the cluster at a higher rate on its negative x side since individual disks, driven by the moving substrate, collide with the negative x side of the cluster and can become trapped in this higher density area. The positive x side of the cluster tends to shed disks at a higher rate since the disks can be carried away by the moving substrate into the low-density gas region. The resulting asymmetric growth rate causes the cluster to drift in the negative x-direction. There is a net overall transport of disks in the positive x-direction due to the large number of gas-phase disks outside of the cluster region that follow the motion of the substrate. Figure 11(a) shows the disk positions at $A_s = 1.0$ and $v_w = 0.4$, where the cluster is drifting in the negative x-direction. For strong substrate strengths, all the disks that are outside of the cluster become strongly confined in the Q1D substrate minima, and the disk density inside the cluster itself starts to become modulated by the substrate. Under these conditions, the cluster is dragged along with the traveling substrate in the positive x-direction, as illustrated in Fig. 11(b) for $A_s = 3.0$ and $v_w = 5.0$. These results suggest that it may be possible for certain active matter systems to collectively form a cluster state in order to move

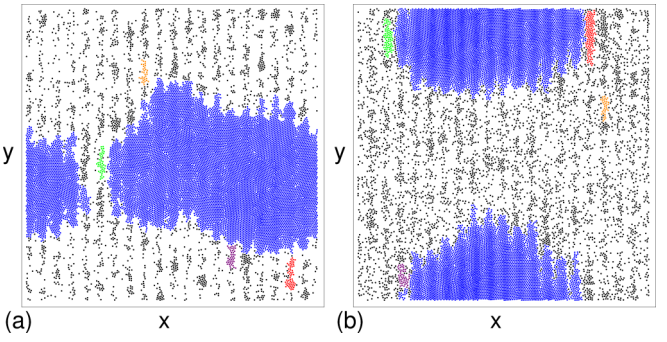

FIG. 11. The disk positions for the system in Figs. 9 and 10. (a) At $A_s = 1.0$ and $v_w = 0.4$, the cluster drifts in the negative x-direction. (b) At $A_s = 3.0$ and $v_w = 5.0$, the cluster drifts in the positive x-direction.

against an external bias even when isolated individual particles on average move with the bias.

V. SUMMARY

We have examined run-and-tumble active matter disks interacting with traveling-wave periodic substrates. We find that in the non-phase-separated state, the disks couple to the traveling waves, and that at the transition to the cluster state there is a partial decoupling from the substrate, and the net transport of disks by the traveling wave is strongly reduced. We also find a transition from a cluster state to a periodic quasi-1D liquid state for increasing substrate strength, as well as a transition back to a cluster state for increasing traveling-wave speed. We show that there is a transition from a noncluster to a cluster state as a function of increasing disk density, which is correlated with a drop in the net disk transport. Since disks with different run times drift with different velocities, our results indicate that traveling-wave substrates could be an effective method for separating active matter particles with different mobilities. Within the regime in which the system forms a cluster state, we find that as a function of wave speed and substrate strength, there are weak substrate regimes where the center of mass of the cluster moves in the opposite direction from that of the traveling wave, while for stronger substrates, the cluster center of mass moves in the same direction as the traveling wave. The reversed cluster motion occurs due to the spatial asymmetry of the rate at which disks leave or join the cluster. This suggests that collective clustering could be an effective method for forming an emergent object that can move against gradients or drifts even when individual disks on average move with the drift.

ACKNOWLEDGMENTS

This work was carried out under the auspices of the NNSA of the U.S. DOE at LANL under Contract No. DE-AC52-06NA25396.

[1] M. C. Marchetti, J. F. Joanny, S. Ramaswamy, T. B. Liverpool, J. Prost, M. Rao, and R. A. Simha, Hydrodynamics of soft active matter, Rev. Mod. Phys. **85**, 1143 (2013).

[2] C. Bechinger, R. Di Leonardo, H. Löwen, C. Reichhardt, G. Volpe, and G. Volpe, Active Brownian particles in complex and crowded environments, Rev. Mod. Phys. **88**, 045006 (2016).

[3] H. C. Berg, *Random Walks in Biology* (Princeton University Press, Princeton, NJ, 1983).

[4] C. Castellano, S. Fortunato, and V. Loreto, Statistical physics of social dynamics, Rev. Mod. Phys. **81**, 591 (2009).

[5] D. Helbing, Traffic and related self-driven many-particle systems, Rev. Mod. Phys. **73**, 1067 (2001).

[6] M. Rubenstein, A. Cornejo, and R. Nagpal, Programmable self-assembly in a thousand-robot swarm, Science **345**, 795 (2014).

[7] M. Mijalkov, A. McDaniel, J. Wehr, and G. Volpe, Engineering Sensorial Delay to Control Phototaxis and Emergent Collective Behaviors, Phys. Rev. X **6**, 011008 (2016).

[8] J. R. Howse, R. A. L. Jones, A. J. Ryan, T. Gough, R. Vafabakhsh, and R. Golestanian, Self-Motile Colloidal Particles: From Directed Propulsion to Random Walk, Phys. Rev. Lett. **99**, 048102 (2007).

[9] J. Palacci, S. Sacanna, A. P. Steinberg, D. J. Pine, and P. M. Chaikin, Living crystals of light-activated colloidal surfers, Science **339**, 936 (2013).

[10] I. Buttinoni, J. Bialk'e, F. Kümmel, H. Löwen, C. Bechinger, and T. Speck, Dynamical Clustering and Phase Separation in Suspensions of Self-Propelled Colloidal Particles, Phys. Rev. Lett. **110**, 238301 (2013).

[11] A. G. Thompson, J. Tailleur, M. E. Cates, and R. A. Blythe, Lattice models of nonequilibrium bacterial dynamics, J. Stat. Mech. (2011) P02029.

[12] C. Reichhardt and C. J. Olson Reichhardt, Active microrheology in active matter systems: Mobility, intermittency, and avalanches, Phys. Rev. E **91**, 032313 (2015).

[13] Y. Fily and M. C. Marchetti, Athermal Phase Separation of Self-Propelled Particles with no Alignment, Phys. Rev. Lett. **108**, 235702 (2012).

[14] G. S. Redner, M. F. Hagan, and A. Baskaran, Structure and Dynamics of a Phase-Separating Active Colloidal Fluid, Phys. Rev. Lett. **110**, 055701 (2013).

[15] M. E. Cates and J. Tailleur, When are active Brownian particles and run-and-tumble particles equivalent? Consequences for motility-induced phase separation, Europhys. Lett. **101**, 20010 (2013).

[16] B. M. Mognetti, A. Saric, S. Angioletti-Uberti, A. Cacciuto, C. Valeriani, and D. Frenkel, Living Clusters and Crystals from Low-Density Suspensions of Active Colloids, Phys. Rev. Lett. **111**, 245702 (2013).

[17] D. Levis and L. Berthier, Clustering and heterogeneous dynamics in a kinetic Monte Carlo model of self-propelled hard disks, Phys. Rev. E **89**, 062301 (2014).

[18] M. E. Cates and J. Tailleur, Motility-induced phase separation, Annu. Rev. Condens. Matter Phys. **6**, 219 (2015).

[19] Cs. Sándor, A. Libál, C. Reichhardt, and C. J. Olson Reichhardt, Dewetting and spreading transitions for active matter on random pinning substrates, arXiv:1608.05323.

[20] C. Reichhardt and C. J. Olson Reichhardt, Active matter transport and jamming on disordered landscapes, Phys. Rev. E **90**, 012701 (2014).

[21] T. Vicsek, A. Czirók, E. Ben-Jacob, I. Cohen, and O. Shochet, Novel Type of Phase Transition in a System of Self-Driven Particles, Phys. Rev. Lett. **75**, 1226 (1995).

[22] O. Chepizhko, E. G. Altmann, and F. Peruani, Optimal Noise Maximizes Collective Motion in Heterogeneous Media, Phys. Rev. Lett. **110**, 238101 (2013).

[23] O. Chepizhko and F. Peruani, Active particles in heterogeneous media display new physics, Eur. Phys. J. Spec. Top. **224**, 1287 (2015).

[24] D. Quint and A. Gopinathan, Topologically induced swarming phase transition on a 2D percolated lattice, Phys. Biol. **12**, 046008 (2015).

[25] G. Volpe, I. Buttinoni, D. Vogt, H. J. Kümmerer, and C. Bechinger, Microswimmers in patterned environments, Soft Matter **7**, 8810 (2011).

[26] P. Galajda, J. Keymer, P. Chaikin, and R. Austin, A wall of funnels concentrates swimming bacteria, J. Bacteriol. **189**, 8704 (2007).

[27] M. B. Wan, C. J. Olson Reichhardt, Z. Nussinov, and C. Reichhardt, Rectification of Swimming Bacteria and Self-driven Particle Systems by Arrays of Asymmetric Barriers, Phys. Rev. Lett. **101**, 018102 (2008).

[28] F. Q. Potiguar, G. A. Farias, and W. P. Ferreira, Self-propelled particle transport in regular arrays of rigid asymmetric obstacles, Phys. Rev. E **90**, 012307 (2014).

[29] N. Koumakis, A. Lepore, C. Maggi, and R. Di Leonardo, Targeted delivery of colloids by swimming bacteria, Nat. Commun. **4**, 2588 (2013).

[30] J. Tailleur and M. E. Cates, Sedimentation, trapping, and rectification of dilute bacteria, Europhys. Lett. **86**, 60002 (2009).

[31] C. J. Olson Reichhardt and C. Reichhardt, Ratchet effects in active matter systems, Annu. Rev. Condens. Matter Phys. **8** (2017).

[32] S.-H. Lee, K. Ladavac, M. Polin, and D. G. Grier, Observation of Flux Reversal in a Symmetric Optical Thermal Ratchet, Phys. Rev. Lett. **94**, 110601 (2005).

[33] V. Blickle, T. Speck, L. Helden, U. Seifert, and C. Bechinger, Thermodynamics of a Colloidal Particle in a Time-dependent Nonharmonic Potential, Phys. Rev. Lett. **96**, 070603 (2006).

[34] M. Rex, H. Löwen, and C. N. Likos, Soft colloids driven and sheared by traveling wave fields, Phys. Rev. E **72**, 021404 (2005).

[35] B. B. Yellen, R. M. Erb, H. S. Son, R. Hewlin, H. Shang, and G. U. Lee, Traveling wave magnetophoresis for high resolution chip based separations, Lab Chip **7**, 1681 (2007).

[36] B. B. Yellen and L. N. Virgin, Nonlinear dynamics of superparamagnetic beads in a traveling magnetic-field wave, Phys. Rev. E **80**, 011402 (2009).

[37] R. Chatterjee, S. Chatterjee, P. Pradhan, and S. S. Manna, Interacting particles in a periodically moving potential: Traveling wave and transport, Phys. Rev. E **89**, 022138 (2014).

[38] A. V. Straube and P. Tierno, Tunable interactions between paramagnetic colloidal particles driven in a modulated ratchet potential, Soft Matter **10**, 3915 (2014).

[39] F. Martinez-Pedrero, P. Tierno, T. H. Johansen, and A. V. Straube, Regulating wave front dynamics from the strongly discrete to the continuum limit in magnetically driven colloidal systems, Sci. Rep. **6**, 19932 (2016).

[40] P. Tierno and A. Straube, Transport and selective chaining of bidisperse particles in a traveling wave potential, Eur. Phys. J. E **39**, 54 (2016).

[41] R. E. Goldstein, Traveling-Wave Chemotaxis, Phys. Rev. Lett. **77**, 775 (1996).

[42] S. Luding and H. J. Herrmann, Cluster-growth in freely cooling granular media, Chaos **9**, 673 (1999).

[43] CGAL library, http://www.cgal.org.